Journal of Molecular Structure 1272 (2023) 134166

Contents lists available at ScienceDirect

Journal of Molecular Structure

journal homepage: www.elsevier.com/locate/molstr

Design, synthesis, and antimicrobial activity of novel coumarin derivatives: An *in-silico* and *in-vitro* study

Demokrat Nuha[a,b,c,*], Asaf Evrim Evren[a,d], Özge Kapusiz[e], Ülküye Dudu Gül[f], Nalan Gundogdu-Karaburun[a], Ahmet Çagri Karaburun[a], Halil Berber[b]

[a] *Faculty of Pharmacy, Department of Pharmaceutical Chemistry, Anadolu University, Eskişehir 26470, Turkey*
[b] *Faculty of Science, Department of Chemistry, Eskisehir Technical University, Eskişehir 26555, Turkey*
[c] *Faculty of Pharmacy, University of Business and Technology, Pristina, Kosovo*
[d] *Vocational School of Health Services, Department of Pharmacy Services, Bilecik Seyh Edebali University, Bilecik 11000, Turkey*
[e] *Graduate School of Education Sciences, Department of Bioengineering, Bilecik Seyh Edebali University, Bilecik 11230, Turkey*
[f] *Faculty of Engineering, Department of Bioengineering, Bilecik Seyh Edebali University, Bilecik 11230, Turkey*

ARTICLE INFO

Article history:
Received 26 June 2022
Revised 7 September 2022
Accepted 15 September 2022
Available online 16 September 2022

Keywords:
Coumarin
Antimicrobial activity
Molecular docking
Molecular dynamics simulation
DFT calculation

ABSTRACT

The novel series of coumarin derivatives have been synthesized, and the chemical structures of the compounds have been elucidated by ^{1}H NMR, ^{13}C NMR, and LC/MS-IT-TOF spectral data. All compounds were tested on eight bacteria and three fungal species, and for each, the minimum inhibitory concentration (MIC) was calculated. Some of the compounds exhibited good activity against microbial strains. Compound **4e** was found to be 2-fold and 4-fold more active against C. *parapsilopsis* (MIC: 0.97 μg/mL) than standard drugs voriconazole and fluconazole, respectively. Compounds **4a** and **4i** also show good activity against E. *faecalis* and E. *coli*, respectively. Compounds **4e** and **4a** were used in molecular docking and dynamic simulation to examine on 14α-demethylase (LDM) and thymidylate synthase (TS). Furthermore, using density functional theory at the B3LYP/6–31 G (d, p) level, the chemical reactivity properties of all molecules were examined.

1. Introduction

Antibiotics have probably been one of the most important and valuable discoveries in the history of medicine since their discovery in 1929. From the first antibiotic, penicillin, through later antibiotics, such as vancomycin and quinolones, usage of them enables mankind to survive pathogens-associated diseases [1]. Antibiotic overuse, unneeded and improper antibiotic usage, and inadequate infection control in hospitals and clinics have all increased selective pressure on bacteria, resulting in the emergence and spread of antimicrobial resistance (AMR) [2]. Antimicrobial resistance has been identified by the World Health Organization (WHO) as one of the key global health issues of the 21st century. Antibiotic resistance causes 700,000 fatalities annually, according to the Centers for Disease Control and Prevention (CDC), with 10 million deaths anticipated by 2050 if current trends continue [3]. In 2017, WHO designated 12 families of antibiotic-resistant bacteria as "superbugs," warning that these bacteria may soon become untreatable by any antimicrobial medication now available [4]. As a result, there is a compelling need to identify and develop new classes of antimicrobial drugs that may successfully treat antimicrobial-resistant bacteria.

Given the increase of AMR and an increasingly limited supply of effective antibiotics, the World Health Organization (WHO) has issued an urgent worldwide call for the development of novel antimicrobial medicines. The new discovery of antimicrobial agents other than traditional antibiotics, such as antimicrobial peptides (AMPs), has an appealing therapeutic use [5,6]. AMPs, also known as host defense peptides, are naturally occurring and/or synthetically modified protein fragments with antibacterial activity [7]. Antimicrobial peptides (AMPs) show extensive antimicrobial action against a variety of microbial pathogens, including gram-positive and gram-negative bacteria, multi-drug resistant (MDR) bacteria, fungi, parasites, and even enveloped viruses [8]. Natural AMPs are typically positively charged, amphipathic, include 12–50 amino acid residues, and interact with bacteria via electrostatic interactions followed by disruption of bacterial membrane structures. The higher content of negatively charged cell wall components in bacterial membranes, such as teichoic acids, cardiolipin, and phosphatidylglycerol, explains the selectivity of cationic AMPs for bac-

* Corresponding author at: Faculty of Pharmacy, Department of Pharmaceutical Chemistry, Anadolu University, Eskişehir 26470, Turkey.
E-mail address: demokrat_nuha@eskisehir.edu.tr (D. Nuha).

https://doi.org/10.1016/j.molstruc.2022.134166
0022-2860/

terial membranes, whereas mammalian cell membranes are composed of neutrally charged phospholipids and are stabilized by cholesterol [9]. Over 3000 natural AMPs have been identified and described so far. In conjunction with a huge number of chemically produced sequences, AMPs would represent a gold mine for the discovery of new antimicrobial drugs. Several AMPs have been licensed for sale, including Daptomycin, Bacitracin, Polimyxin B, Colistin, Tyrothricin, and Gramicidin, and at least 20 others are in the application or clinical development stages [10].

Coumarins are well-known chemical entities with unique qualities such as simple structure, high solubility, good bioavailability, low toxicity, and so on, and may be found in a broad variety of plant-derived goods and nutraceuticals. Because of their various biological and pharmacological effects, natural and synthesized coumarins have aroused the curiosity of researchers. These are linked to a variety of biological processes, including antibacterial activity [11], antifungal [12,13], antioxidant [14], antitumor [15], anticancer [16], anti-inflammatory [17], anticoagulant [18], antihypertensive [19], antitubercular [20], and antidepressant [21], etc.

Based on all of this information, we set out to create a new series of physiologically active compounds featuring this essential pharmacophore. The synthesis, characterization, molecular docking studies, molecular dynamics simulation studies, DFT calculation, and *in vitro* antimicrobial properties of these novel coumarin derivatives are described in this paper.

2. Experimental

2.1. Chemistry

All chemicals used in the syntheses were purchased either from Merck Chemicals (Merck KGaA, Darmstadt, Germany) or Sigma-Aldrich Chemicals (Sigma-Aldrich Corp., St. Louis, MO, USA). The reactions and the purities of the compounds were observed by thin-layer chromatography (TLC) on silica gel 60 F254 aluminum sheets obtained from Merck (Darmstadt, Germany). The melting points of the synthesized compounds were recorded by the MP90 digital melting point apparatus (Mettler Toledo, Ohio, USA) and were presented as uncorrected. ^{1}H NMR and ^{13}C NMR spectral analyses were achieved using a Bruker 300 MHz and 75 MHz digital FT-NMR spectrometer (Bruker Bioscience, Billerica, MA, USA) in DMSO–d_6. In the NMR spectra, splitting patterns were designated as follows: s: singlet; d: doublet; t: triplet; m: multiplet. Coupling constants (*J*) were reported as Hertz. High resolution mass spectrometric (HRMS) analyses were performed using a LC/MS-IT-TOF system (Shimadzu, Kyoto, Japan).

2.1.1. General synthesis of ethyl 2-[(2-oxo-2H-chromen-4-yl)oxy]acetate (1)

4-Hydroxy-2*H*-chromen-2-one (0.02 mol, 3.24 g) was mixed with ethyl 2-bromoacetate (0.024 mol, 2.67 mL) and potassium carbonate (0.03 mol, 4.15 g). The mixture was heated in acetone (150 mL) for 12 h. The solvent was evaporated after TLC analysis, and the material was filtered and washed with water before being recrystallized from ethanol.

2.1.2. General synthesis of 2-[(2-oxo-2H-chromen-4-yl)oxy]acetohydrazide (2)

Ethyl 2-[(2-oxo-2*H*-chromen-4-yl)oxy]acetate (**1**) (0.017 mol, 4.33 g) and hydrazine hydrate (0.1 mol of 85%) were stirred at room temperature in ethanol (150 mL). After control using TLC, stirring was stopped and the mixture was awaited till two phases of solvent and precipitate were formed. The precipitated material was filtered. After drying, the product was recrystallized from ethanol.

2.1.3. General synthesis of 2-{2-[(2-oxo-2H-chromen-4-yl)oxy]acetyl}-N-phenylhydrazinecarbothioamide (3)

2-[(2-Oxo-2*H*-chromen-4-yl)oxy]acetohydrazide (**2**) (0.012 mol, 3 g) and isothiocyanatobenzene (0.012 mol, 1.73 g) were refluxed in ethanol (100 mL) for 3 h. TLC was used to observe the reaction. The solvent was evaporated, and the scraped material was removed. The raw product was recrystallized from ethanol.

2.1.4. General synthesis of N'-[3,4-diphenylthiazol-2(3H)-ylidene]–2-[(2-oxo-2H-chromen-4-yl)oxy]acetohydrazide derivatives (4a–4j)

The synthesized intermediates 2-{2-[(2-oxo-2*H*-chromen-4-yl)oxy]acetyl}-*N*-phenylhydrazinecarbothioamide (**3**) (0.81 mmol, 0.3 g) were refluxed with phenacyl bromide derivatives (0.81 mmol) for 12 h in ethanol. After overnight standing in a cool place, crystals of the final thiazole compounds were filtered off.

2.1.5. N'-(3,4-Diphenylthiazol-2(3H)-ylidene)–2-[(2-oxo-2H-chromen-4-yl)oxy]acetohydrazide (4a)

m. p. 194–195 °C, yield 72%, ^{1}H NMR (300 MHz, DMSO–d_6, ppm) δ 5.10 (s, 2H, acetohydrazide-$\underline{CH_2}$), 5.80 (s, 1H, chromen-2-one-$\underline{C_3}$), 7.18 (d, J = 5.98 Hz, 1H, Ar-H), 7.25–7.33 (m, 2H, Ar-H), 7.42–7.50 (m, 7H, Ar-H), 7.56–7.63 (m, 3H, Ar-H), 7.68–7.75 (m, 1H, Ar-H), and 7.94–8.03 (m, 1H, Ar-H). ^{13}C NMR (75 MHz, DMSO–d_6, ppm) δ 67.34 (acetohydrazide-$\underline{CH_2}$), 92.10 (chromen-2-one-$\underline{C_3}$), 115.09, 116.89, 123.90, 124.15, 124.68, 127.50, 128.80, 128.99, 129.23, 129.65, 130.42, 130.93, 133.55, 134.94, 140.99, 142.10, 153.13, 153.17, 161.63, 164.22, 165.29, and 166.14. HRMS (*m/z*): $[M + H]^+$ calculated 470.1169; found 470.1150.

2.1.6. N'-[4-(4-Fluorophenyl)–3-phenylthiazol-2(3H)-ylidene]–2-[(2-oxo-2H-chromen-4-yl)oxy]acetohydrazide (4b)

m. p. 215–216 °C, yield 80%, ^{1}H NMR (300 MHz, DMSO–d_6, ppm) δ 5.06 (s, 2H, acetohydrazide-$\underline{CH_2}$), 5.89 (s, 1H, chromen-2-one-$\underline{C_3}$), 7.11 (t, J = 8.91 Hz, 3H, Ar-H), 7.26 (t, J = 6.89 Hz, 2H, Ar-H), 7.41–7.46 (m, 6H, Ar-H), 7.57 (t, J = 5.97 Hz, 1H, Ar-H), 7.69 (s, 1H, Ar-H), and 7.91–8.02 (m, 1H, Ar-H). ^{13}C NMR (75 MHz, DMSO–d_6, ppm) δ 67.74 (acetohydrazide-$\underline{CH_2}$), 92.55 (chromen-2-one-$\underline{C_3}$), 105.35, 116.19, 116.48, 117.38, 124.36, 125.19, 129.33, 130.86, 131.35, 132.68, 133.99, 135.49, 141.40, 153.65, 162.29, 165.20, 165.54, 166.69, and 172.24. HRMS (*m/z*): [M + H]+ calculated 488.1075; found 488.1054.

2.1.7. N'-[4-(4-Nitrophenyl)–3-phenylthiazol-2(3H)-ylidene]–2-[(2-oxo-2H-chromen-4-yl)oxy]acetohydrazide (4c)

m. p. 212–213 °C, yield 85%, ^{1}H NMR (300 MHz, DMSO–d_6, ppm) δ 4.98 (s, 2H, acetohydrazide-$\underline{CH_2}$), 5.54 and 5.89 (s, 1H, chromen-2-one-$\underline{C_3}$), 7.12–7.29 (m, 1H, Ar-H), 7.38–7.52 (m, 8H, Ar-H), 7.69 (t, J = 7.93 Hz, 1H, Ar-H), 7.78 (d, J = 8.45 Hz, 1H, Ar-H), 7.91–8.02 (m, 1H, Ar-H), 8.10 (d, J = 8.47 Hz, 1H, Ar-H), 8.24 (d, J = 8.32 Hz, 1H, Ar-H), and 10.95 (brs, 1H, -$\underline{NH}$). ^{13}C NMR (75 MHz, DMSO–d_6, ppm) δ 67.75 (acetohydrazide-$\underline{CH_2}$), 92.12 (chromen-2-one-$\underline{C_3}$), 106.10, 117.17, 123.19, 124.19, 124.55, 124.97, 129.13, 130.04, 130.42, 130.59, 130.88, 133.75, 139.29, 147.95, 162.13, 165.09, and 166.31. HRMS (*m/z*): [M + H]+ calculated 515.1020; found 515.0999.

2.1.8. N'-[4-(4-Chlorophenyl)–3-phenylthiazol-2(3H)-ylidene]–2-[(2-oxo-2H-chromen-4-yl)oxy]acetohydrazide (4d)

m. p. 230–231 °C, yield 82%, ^{1}H NMR (300 MHz, DMSO–d_6, ppm) δ 5.00 (s, 2H, acetohydrazide-$\underline{CH_2}$), 5.81 (s, 1H, chromen-2-one-$\underline{C_3}$), 6.96 (s, 1H, Ar-H), 7.27–7.36 (m, 2H, Ar-H), 7.42–7.47 (m, 3H, Ar-H), 7.48–7.56 (m, 6H, Ar-H), 7.71 (t, J = 7.33 Hz, 1H, Ar-H), 7.94 (d, J = 7.99 Hz, 1H, Ar-H), and 11.98 (brs, 1H, -$\underline{NH}$). ^{13}C NMR (75 MHz, DMSO–d_6, ppm) δ 67.53 (acetohydrazide-$\underline{CH_2}$), 92.45 (chromen-2-one-$\underline{C_3}$), 115.38, 117.19, 123.49, 124.06, 124.93, 127.40,

129.57, 130.66, 130.91, 131.46, 133.75, 135.49, 139.51, 153.39, 161.85, 164.51, and 166.54. HRMS (m/z): [M + H]+ calculated 504.0779; found 504.0785.

2.1.9. N'-[4-(4-Cyanophenyl)−3-phenylthiazol-2(3H)-ylidene]−2-[(2-oxo-2H-chromen-4-yl)oxy]acetohydrazide (4e)

m. p. 233–234 °C, yield 79%, ^{1}H NMR (300 MHz, DMSO–d_6, ppm) δ 5.04 (s, 2H, acetohydrazide-$\underline{CH_2}$), 5.70 (s, 1H, chromen-2-one-$\underline{C_3}$), 7.14 (s, 1H, Ar-H), 7.33 (t, J = 7.15 Hz, 3H, Ar-H), 7.42–7.47 (m, 2H, Ar-H), 7.53 (t, J = 7.43 Hz, 2H, Ar-H), 7.73 (d, J = 8.22 Hz, 3H, Ar-H), 7.87–7.95 (m, 3H, Ar-H), and 12.10 (brs, 1H, -$\underline{NH}$). ^{13}C NMR (75 MHz, DMSO–d_6, ppm) δ 67.21 (acetohydrazide-$\underline{CH_2}$), 92.06 (chromen-2-one-$\underline{C_3}$), 102.68, 112.90, 115.12, 116.93, 118.74, 121.21, 123.22, 123.82, 124.71, 127.13, 129.31, 130.30, 130.69, 132.51, 133.10, 133.55, 138.82, 153.12, 161.53, 164.28, and 166.34. HRMS (m/z): $[M + H]^+$ calculated 495.1122; found 495.1112.

2.1.10. 2-[(2-Oxo-2H-chromen-4-yl)oxy]-N'-[3-phenyl-4-(p-tolyl)thiazol-2(3H)-ylidene]acetohydrazide (4f)

m. p. 232–233 °C, yield 86%, ^{1}H NMR (300 MHz, DMSO–d_6, ppm) δ 2.31 (s, 3H, Ar-$\underline{CH_3}$), 4.99 (s, 2H, acetohydrazide-$\underline{CH_2}$), 5.75 (s, 1H, chromen-2-one-$\underline{C_3}$), 6.92–7.02 (m, 1H, Ar-H), 7.20 (d, J = 7.99 Hz, 2H, Ar-H), 7.38–7.46 (m, 7H, Ar-H), 7.54 (t, J = 6.81 Hz, 2H, Ar-H), 7.71 (t, J = 7.25 Hz, 1H, Ar-H), 7.95 (d, J = 7.99 Hz, 1H, Ar-H), and 12.07 (brs, 1H, -$\underline{NH}$). ^{13}C NMR (75 MHz, DMSO–d_6, ppm) δ 21.40 (Ar-$\underline{CH_3}$), 67.29 (acetohydrazide-$\underline{CH_2}$), 92.13 (chromen-2-one-$\underline{C_3}$), 115.14, 116.90, 121.30, 123.56, 123.86, 124.66, 128.61, 129.74, 130.22, 130.76, 133.53, 140.32, 153.14, 161.55, 164.22, and 166.17. HRMS (m/z): [M + H]$^+$ calculated 484.1326; found 484.1317.

2.1.11. N'-[4-(4-Methoxyphenyl)−3-phenylthiazol-2(3H)-ylidene]−2-[(2-oxo-2H-chromen-4-yl)oxy]acetohydrazide (4 g)

m. p. 236–237 °C, yield 77%, ^{1}H NMR (300 MHz, DMSO–d_6, ppm) δ 3.79 (s, 3H, Ar–O$\underline{CH_3}$), 5.01 (s, 2H, acetohydrazide-$\underline{CH_2}$), 5.80 (s, 1H, chromen-2-one-$\underline{C_3}$), 6.98 (d, J = 8.79 Hz, 3H, Ar-H), 7.39–7.47 (m, 7H, Ar-H), 7.54 (d, J = 6.99 Hz, 2H, Ar-H), 7.71 (t, J = 6.71 Hz, 1H, Ar-H), 7.95 (t, J = 7.99 Hz, 1H, Ar-H), and 12.09 (brs, 1H, -$\underline{NH}$). ^{13}C NMR (75 MHz, DMSO–d_6, ppm) δ 55.68 (Ar–O$\underline{CH_3}$), 67.28 (acetohydrazide-$\underline{CH_2}$), 92.18 (chromen-2-one-$\underline{C_3}$), 114.36, 114.63, 115.14, 116.93, 121.31, 123.84, 124.65, 130.22, 130.32, 130.77, 131.28, 133.53, 153.15, 160.92, 161.64, 164.28, and 166.20. HRMS (m/z): [M + H]+ calculated 500.1275; found 500.1270.

2.1.12. N'-(4-(3-Chlorophenyl)−3-phenylthiazol-2(3H)-ylidene)−2-((2-oxo-2H-chromen-4-yl)oxy)acetohydrazide (4 h)

m. p. 100–101 °C, yield 80%, ^{1}H NMR (300 MHz, DMSO–d_6, ppm) δ 5.05 (s, 2H, acetohydrazide-$\underline{CH_2}$), 5.90 (s, 1H, chromen-2-one-$\underline{C_3}$), 7.17 (d, J = 8.10 Hz, 1H, Ar-H), 7.26–7.34 (m, 2H, Ar-H), 7.41–7.54 (m, 8H, Ar-H), 7.69 (d, J = 7.66 Hz, 1H, Ar-H), 7.85 (d, J = 7.82 Hz, 1H, Ar-H), 8.00 (t, J = 8.07 Hz, 1H, Ar-H), and 11.15 (brs, 1H, -$\underline{NH}$). ^{13}C NMR (75 MHz, DMSO–d_6, ppm) δ 67.33 (acetohydrazide-$\underline{CH_2}$), 92.06 (chromen-2-one-$\underline{C_3}$), 105.26, 115.32, 116.90, 123.64, 123.90, 124.71, 128.20, 128.87, 129.33, 130.32, 130.59, 130.81, 131.46, 133.50, 135.27, 140.10, 153.18, 161.83, 164.74, 166.21, and 171.34. HRMS (m/z): [M + H]$^+$ calculated 504.0779; found 504.0756.

2.1.13. N'-(4-(3-Nitrophenyl)−3-phenylthiazol-2(3H)-ylidene)−2-((2-oxo-2H-chromen-4-yl)oxy)acetohydrazide (4i)

m. p. 175–176 °C, yield 85%, ^{1}H NMR (300 MHz, DMSO–d_6, ppm) δ 5.09 (s, 2H, acetohydrazide-$\underline{CH_2}$), 5.91 (s, 1H, chromen-2-one-$\underline{C_3}$), 7.29–7.37 (m, 2H, Ar-H), 7.40–7.44 (m, 4H, Ar-H), 7.53–7.61 (m, 2H, Ar-H), 7.68–7.78 (m, 2H, Ar-H), 7.84–8.01 (m, 2H, Ar-H), 8.12–8.23 (m, 1H, Ar-H), 8.32–8.47 (m, 1H, Ar-H), and 11.29 (brs, 1H, -$\underline{NH}$). ^{13}C NMR (75 MHz, DMSO–d_6, ppm) δ 65.85 (acetohydrazide-$\underline{CH_2}$), 90.82 (chromen-2-one-$\underline{C_3}$), 115.82, 118.01, 122.33, 122.76, 123.22, 123.60, 124.49, 125.82, 127.82, 128.36, 129.30, 129.76, 130.01, 131.53, 131.81, 131.92, 132.04, 132.41, 134.54, 153.12, 161.54, 161.82, and 164.65. HRMS (m/z): [M + H]+ calculated 515.1020; found 515.0997.

2.1.14. N'-{4-[4-(Methylsulfonyl)phenyl]−3-phenylthiazol-2(3H)-ylidene}−2-[(2-oxo-2H-chromen-4-yl)oxy]acetohydrazide (4j)

m. p. 214–215 °C, yield 74%, ^{1}H NMR (300 MHz, DMSO–d_6, ppm) δ 3.29 (s, 3H, SO_2-$\underline{CH_3}$), 5.04 (s, 2H, acetohydrazide-$\underline{CH_2}$), 5.79 (s, 1H, chromen-2-one-$\underline{C_3}$), 7.03 (s, 1H, Ar-H), 7.22–7.30 (m, 3H, Ar-H), 7.41–7.51 (m, 5H, Ar-H), 7.70 (t, J = 7.31 Hz, 1H, Ar-H), 7.80 (d, J = 8.35 Hz, 2H, Ar-H), 7.99 (t, J = 7.98 Hz, 2H, Ar-H), and 11.89 (brs, 1H, -$\underline{NH}$). ^{13}C NMR (75 MHz, DMSO–d_6, ppm) δ 43.65 (SO_2-$\underline{CH_3}$), 67.22 (acetohydrazide-$\underline{CH_2}$), 92.23 (chromen-2-one-$\underline{C_3}$), 116.93, 122.77, 123.86, 124.72, 127.58, 127.88, 129.09, 129.63, 130.54, 133.54, 138.61, 141.90, 153.13, 161.69, 164.41, and 166.50. HRMS (m/z): [M + H]$^+$ calculated 548.0945; found 548.0933.

2.2. Antimicrobial activity

The antimicrobial activity of final compounds (**4a–4j**) was screened on eight bacterial and three fungal strains according to the standard procedure of CLSI [22] as described in the previous study [23,24]. The antibacterial activities of the synthesized compounds were tested against *Escherichia coli* (ATCC 25,922), *Serratia marcescens* (ATCC 8100), *Klebsiella pneumoniae* (ATCC 13,883), *Pseudomonas aeruginosa* (ATCC 27,853), *Enterococcus faecalis* (ATCC 2942), *Bacillus subtilis* (ATCC 6633), *Staphylococcus aureus* (ATCC 29,213), *and Staphylococcus epidermidis* (ATCC 12,228). *Candida albicans* (ATCC 24,433), *Candida krusei* (ATCC 6258), and *Candida parapsilopsis* (ATCC 22,019) were used to test the antifungal activity of the same compounds. Azithromycin (against bacterial strains), Voriconazole, and fluconazole (against candida strains) were used as standard reference drugs.

2.3. ADME parameters

The prediction of the physicochemical parameters of compounds (**4a–4j**) was calculated using the SwissADME web-based program [25–27].

2.4. In silico *studies*

The crystal structures of the lanosterol 14α-demethylase (LDM) and *E. faecalis* thymidylate synthase enzymes were retrieved from the Protein Data Bank server (PDB codes: 5TZ1 and 5J7W). The protein preparation process, ligand preparation process, grid generation, docking, and visualization studies were performed on Schrodinger's Maestro molecular modeling package [28]. Ligands were set to the physiological pH (pH = 7.4 ± 1.0) at the protonation step. In molecular docking simulations: Glide/SP docking protocols were applied to determine the binding modes (between 4a and thymidylate synthase; 4e and LDM enzyme active regions). After the preparation steps, the molecules were docked to the active region of the related enzyme. The docking study was used here to predict the relationship between the structures and inhibition activity of the enzymes. After the determination of the best poses, docking studies were discussed, and then the best poses were carried on to the next step, molecular dynamics simulation studies, which were performed to determine the stability of the complexes during time. MD simulation for 100 ns were carried out to ensure the stability of the identified hits from the docking result. We performed the Desmond application [29] using the standard force field (OPLS3e) of the Schrodinger Suite with a transferable intermolecular potential with a 3 points (TIP3P) water model followed by energy minimization of the complex. The neutralization of the system

was achieved using Na^+ and Cl^- ions to provide a final salt concentration of 0.15 M in order to simulate physiological concentration of monovalent ions. Constant temperature (300 K) and pressure (1.01325 bar) were employed with NPT (constant number of particles, pressure, and temperature) as ensemble class. RESPA integrator [30] was used in order to integrate the equations of motion. NH thermostats [31] were used to keep the constant simulation temperature, and the MTK method [32] was applied to control the pressure. Long-range electrostatic interactions were calculated by pmE method [33]. The cutoff for van der Waals and short-range electrostatic interactions was set at 9.0 Å. The equilibration of the system was performed with the default protocol provided in Desmond, which consists of a series of restrained minimizations and molecular dynamics simulations used to slowly relax the system. This procedure was also previously applied by *in silico* study group [34]. The MD simulation was performed using above settings and following the completion of the system setup. Rg (radius of gyration), root mean square fluctuation (RMSF) and root mean square deviation (RMSD) values were calculated by the Desmond application. In the end, the results were used to build a structure-activity relationship (SAR).

2.5. Theoretical details

The Gaussian 09 W package [35] and GaussView 5.0 [36] molecular visualization programs were used to perform theoretical approaches for *N'*-(3,4-diphenylthiazol-2(3*H*)-ylidene)−2-[(2-*oxo*-2*H*-*chromen*-4-*yl*)*oxy*]acetohydrazide derivatives (**4a–4j**). Density Functional Theory (DFT), Becke's Three-Parameter Hybrid Functional using the Lee, Yang, and Parr correlation (B3LYP) [37] method with 6–31 G (d, p) basis set in the ground state and gas phase were used to optimize the compounds' geometry. The highest occupied molecular orbital (HOMO) and lowest unoccupied molecular orbital (LUMO) energy values of the groups of compounds were obtained at a time-dependent (TD)-DFT level to describe intramolecular charge-transfer interactions.

HOMO-LUMO energy values were used to calculate chemical activity parameters such as I; ionization potential ($I = -E_{HOMO}$), A; electron affinity ($A = -E_{LUMO}$), χ;electronegativity ($\chi = (I + A)/2$), η;chemical hardness (η = (I-A)/2), S; chemical softness ($S = 1/2\eta$), μ; chemical potential ($\mu = -(I + A)/2$) and ω;electrophilicity index ($\omega = \mu^2/2\eta$) of the molecular groups [38].

3. Results and discussion

3.1. Chemistry

The compounds **4a–4j** were synthesized as summarized in Scheme 1.

Initially, the ethyl 2-[(2-*oxo*-2*H*-*chromen*-4-*yl*)*oxy*]acetate (**1**) resulted from the reaction of 4–hydroxy-2*H*-chromen-2-one with ethyl 2-bromoacetate. Then, the obtained compound **1** was treated with hydrazine hydrate to gain 2-[(2-*oxo*-2*H*-*chromen*-4-*yl*)*oxy*]acetohydrazide (**2**). Then, obtained compound **2** was first treated with isothiocyanatobenzene to synthesized 2-{2-[(2-*oxo*-2*H*-*chromen*-4-*yl*)*oxy*]acetyl}-*N*-phenylhydrazinecarbothioamide (**3**) and those products were treated with phenacyl bromide derivatives to gain *N'*-[3,4-*diphenylthiazol*-2(3*H*)-*ylidene*]−2-[(2-*oxo*-2*H*-*chromen*-4-*yl*)*oxy*]acetohydrazide derivatives (**4a–4j**) as the core structure. The structures of the final compounds (**4a–4j**) were confirmed by ^{1}H NMR, ^{13}C NMR, and high-resolution mass spectroscopy (HRMS).

3.1.1. NMR spectrum

In the ^{1}H NMR and ^{13}C NMR spectra, the peaks were observed at estimated aromatic and aliphatic regions. The mass peaks [M + 1] of the compounds were in agreement with their predicted molecular formula (**4a–4j**).

The ^{1}H NMR spectra showed signals at δ 4.98–5.10 ppm for acetohydrazide-$\underline{CH_2}$ protons, which were singlet peaks. Chromen-2-one-$\underline{C_3}$ proton was observed at δ 5.54–5.91 ppm ($\underline{CH}$) as singlet peaks. A broad singlet peak seen at δ 10.95–12.10 ppm indicated the acetamide N–H proton. The appearance of a pair of singlets, doublets, triplets, and/or multiplets δ 6.92–8.47 ppm were due to the aromatic protons of the aromatic rings. The ^{13}C NMR spectra showed signals at δ 65.85–67.75 ppm for acetohydrazide-$\underline{CH_2}$ carbon, while those at δ 90.82–92.55 ppm was for chromen-2-one-$\underline{C_3}$ carbon, δ 102.68–166.69 ppm for aromatic carbon, and δ 164.65–172.24 ppm for carbonyl (C = O) carbon. The $M + 1$ peaks in the LC-MS/MS spectra were in agreement with the calculated molecular weight of the target compounds (**4a–4j**).

3.2. ADME parameters

In silico ADME (Absorption, Distribution, Metabolism, and Excretion) research of molecules **4a–4j** was performed using the SwissADME online tool, and important 5 physicochemical characteristics were calculated [39,40]. The values of HBA, HBD, TPSA, Log P, Log S, Log K, GIA, and other parameters are depicted in Table 1. On the basis of the Lipinski "Rule of 5′′, all the prepared compounds have good membrane permeability (BBB/GI), log P (3.60–4.92) ≤5, number of hydrogen bond acceptors (5–7) ≤10, and the number of hydrogen bond donors (1) ≤5 [41,42]. The pharmacophore or drug-like features of the compounds demonstrate that they all adhere to and fulfill the Lipinski rule, with all attributes falling within an acceptable range. These findings are consistent with the compounds' potential for action. The pharmacokinetic profile of the produced compounds is predicted to be good. As a consequence, the drug-likeness of the compounds was recognized as a positive.

3.3. Antimicrobial activity

There has been antimicrobial research on coumarin derivatives, and they are also more appealing for removing invasive microbes and have fewer side effects than other derivatives [43–45]. As a consequence, the core structure of the final molecules was synthesized in this work based on this superiority.

3.3.1. Anticandidal activity

The final compounds (**4a–4j**) were tested against *Candida albicans* (ATCC 24,433*), Candida krusei* (ATCC 6258), and *Candida parapsilopsis* (ATCC 22,019*)*. The results are showed in Table 2.

Based on the results, compound **4e** (MIC: 0.97 µg/mL against *C. parapsilopsis*) was found to be 2-fold and 4-fold more active than standard drugs voriconazole and fluconazole, respectively. With regard to the activity against *C. albicans*, there was no compound worthy of note as an antifungal drug except **4i** (MIC: 15.63 µg/mL). The standard drugs voriconazole and fluconazole were found to be 4-fold and 2-fold more active, respectively, than compound **4i**. While the activity potential of other compounds as anticandidal was found to be modest, they may be useful as a basis to develop anticandidal drugs.

3.3.2. Antibacterial activity

The final compounds (**4a–4j**) were tested against *E. coli* (ATCC 25,922), *Serratia marcescens* (ATCC 8100), *Klebsiella pneumoniae* (ATCC 13,883), *Pseudomonas aeruginosa* (ATCC 27,853), *Enterococcus faecalis* (ATCC 2942), *Bacillus subtilis* (ATCC 6633), *Staphylococcus aureus* (ATCC 29,213), and *Staphylococcus epidermidis* (ATCC 12,228). The results are shown in Table 3.

According to the results of the *in vitro* study, the final compounds showed modest potency. In general, the MIC values of the

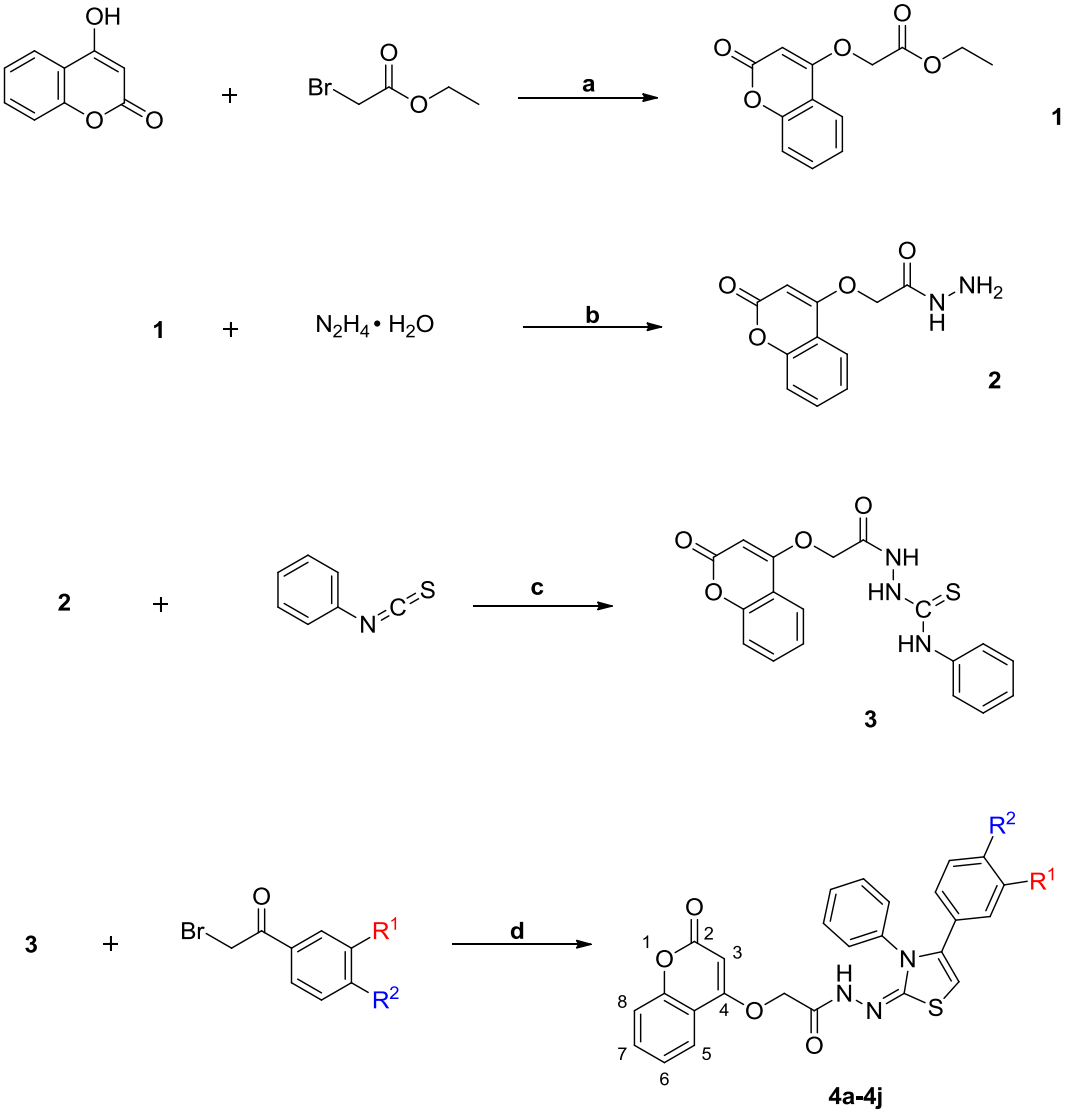

Compounds	R^1	R^2
4a	/	-H
4b	/	-F
4c	/	$-NO_2$
4d	/	-Cl
4e	/	-CN
4f	/	$-CH_3$
4g	/	$-OCH_3$
4h	-Cl	/
4i	$-NO_2$	/
4j	/	$-SO_2CH_3$

Scheme 1. The synthesis diagram of the compounds **4a–4j**. Reagents and conditions: (a) K_2CO_3, acetone, ref., 12 h; (b) EtOH, 0–5 °C, then r.t 8 h; (c) EtOH, ref., 3 h; (d) EtOH, ref., 12 h.

tested compounds were within the range of 1.95–250 μg/mL. However, compound **4i** against *E. coli* (ATCC 25,922) was found active at 3.90 µg/mL and has a 4-fold or 16-fold higher potency than other compounds. Also, the inhibition activity of compound **4a** (MIC:1.95 µg/mL) has a 4-fold or 32-fold higher potency than other compounds against *E. faecalis* (ATCC 2942).

However, compound **4c** against *P. aeruginosa* (ATCC 27,853), *B. subtilis* (ATCC) and *S. aureus* (ATCC 29,213) and compound **4h** against *S. marcescens* (ATCC 8100) and *K. pneumoniae* (ATCC 13,883), were found active at 62.50 µg/mL. As well, compound **4e** against *S. marcescens* (ATCC 8100) and *S. epidermidis* (ATCC 12,228) and compounds **4d** and **4i** against *S. marcescens* (ATCC 8100) were found active at 62.50 µg/mL. There were no variations in the potency of the compounds tested against gram-positive (+) and gram-negative (-) bacteria.

As a straightforward assumption concerning antimicrobial results, the resulting compounds demonstrated modest activity against invasive bacteria and fungi. Alternatively, because the

Table 1
Physicochemical, pharmacokinetic, and medicinal chemistry properties of the final compounds (by SwissAdme) **4a–4j**.

	Physicochemical Properties					Pharmacokinetics		Medicinal Chemistry	
	HBA	HBD	TPSA	Log $P_{o/w}$	Log S	GIA	Log K_p	RoF (V)	SA
4a	5	1	114.07	4.39	−6.96	High	−5.73	Yes (0)	3.94
4b	6	1	114.07	4.67	−7.06	High	−5.77	Yes (0)	3.93
4c	7	1	159.89	3.60	−7.74	Low	−6.13	Yes (1)	4.03
4d	5	1	114.07	4.90	−7.61	High	−5.50	Yes (1)	3.92
4e	6	1	137.86	4.08	−7.17	Low	−6.09	Yes (0)	4.00
4f	5	1	114.07	4.72	−7.33	High	−5.56	Yes (0)	4.05
4g	6	1	123.30	4.30	−7.12	Low	−5.94	Yes (0)	4.09
4h	5	1	114.07	4.92	−7.61	High	−5.50	Yes (1)	3.91
4i	7	1	159.89	3.60	−7.74	Low	−6.13	Yes (1)	4.06
4j	7	1	156.59	4.03	−7.06	Low	−6.75	Yes (1)	4.14
RF-1	8	1	76.72	2.40	−2.73	High	−7.36	Yes (0)	3.61
RF-2	7	1	81.65	0.88	−1.63	High	−7.92	Yes (0)	2.91
RF-3	14	5	180.08	2.08	−7.50	Low	−8.01	No (2)	8.91

HBA: H-bond acceptor, HBD: H-bond donor, TPSA: Topologic polar surface area (Å²) Log $P_{o/w}$: *Consensus* Log $P_{o/w}$ (Average of all five predictions), Log S: Water Solubility, GIA: Gastrointestinal absorption, Log K_p: skin permeation (cm/s) RoF (V): Rule of Five (violation number), SA: Synthetic accessibility from 1 (very easy) to 10 (very difficult). RF- 1: Voriconazole, RF-2: Fluconazole, RF-3: Azithromycin.

Table 2
Antifungal activity of the compounds (**4a–4j**) as MIC values (μg/mL).

	A	B	C
4a	62.5	125	62.5
4b	125	125	62.5
4c	62.5	62.5	31.25
4d	>250	250	125
4e	62.5	250	0.97
4f	62.5	125	125
4g	125	125	125
4h	125	125	62.5
4i	15.625	125	62.5
4j	31.25	125	125
S. D. 1	3.90	3.90	1.95
S. D. 2	7.81	7.81	3.90

A: *C. albicans* (ATCC 24,433), B: *C. krusei* (ATCC 6258), C: *C. parapsilopsis* (ATCC 22,019), S.D.1: Standard Drug = Voriconazole, S.D.2: Standard Drug = Fluconazole.

coumarin ring system allows for substitution variation, it is critical to provide recommendations for future research, namely the structure-activity link (SAR).

3.4. In silico *studies*

3.4.1. Molecular docking studies

After determination of the active compounds against pathogenic microorganisms, the docking studies were performed to understand the binding modes and then to build-up SAR. According to *in vitro* results, the most active compound was **4e** against *C. parapsilosis* and **4a** against *E. faecalis*, hence, the activity pathways should be shaped via them.

Even though lanosterol 14α-demethylase enzyme is known as a common protein for the fungal organism, the drugs are used clinically to show their potency via this enzyme. Also, our compounds include thiazole rings similar to some antifungal drugs such as isavuconazole and ravuconazole. Because of these reasons, we targeted lanosterol 14α-demethylase to dock compound **4e** (Fig. 1). The docking study results showed that, compound **4e** fit well into active side of the enzyme. Moreover, coumarin group interacted various π-π interactions and more importantly π-cation interaction with the HEM's aromatic rings and Fe^{+2} atom of HEM. Addition to that, there were one direct H-bond and three aromatic H-bonds observed between cyano nitrogen and hydroxy group of Ser378; hydrazide oxygen and phenyl H_3 of Phe126; phenyl H_3 and Met508 oxygen; and phenyl H_5 and Ser378 oxygen, respectively. Also, we observed 2 connections with Tyr118 which occurred as π-π stacking and π-cation interaction. All these named residues were reported as pivotal for inhibition activity [46], so the docking study suggests that the action mechanism of this compound is based on inhibiting the LDM enzyme.

Because the activity was found to be specific against the *E. faecalis* strain, the activity mechanism should be related to this bacterium. Therefore, inhibition of the thymidylate synthase enzyme may be a possible mechanism. There are 3 reasons to support this argument: First of all, in a previous study, thymidylate syn-

Table 3
Antibacterial activity of the compounds (**4a–4j**) as MIC values (μg/mL).

	A	B	C	D	E	F	G	H
4a	15.625	125	125	125	1.95	125	125	250
4b	15.625	125	125	125	62.5	125	125	125
4c	15.625	125	125	62.5	7.81	62.5	62.5	125
4d	31.25	62.5	125	125	7.81	125	125	250
4e	15.625	62.5	125	125	7.81	125	125	62.5
4f	15.625	125	125	125	62.5	125	250	125
4g	62.5	125	125	125	62.5	125	250	125
4h	15.625	62.5	62.5	125	7.81	125	125	125
4i	3.90	62.5	125	125	15.625	125	250	125
4j	15.625	125	125	125	3.90	125	250	125
S. D. 1	< 0.97	< 0.97	< 0.97	< 0.97	< 0.97	< 0.97	< 0.97	< 0.97

A: *E. coli* (ATCC 25,922), B: *S. marcescens* (ATCC 8100), C: *K. pneumoniae* (ATCC 13,883), D: *P. aeruginosa* (ATCC 27,853), E: *E. faecalis* (ATCC 2942), F: *B. subtilis* (ATCC), G: *S. aureus* (ATCC 29,213), H: *S. epidermidis* (ATCC 12,228) A-D: Gram negative bacteria, E-H: Gram positive bacteria. S.D: Standard Drug = Azithromycin.

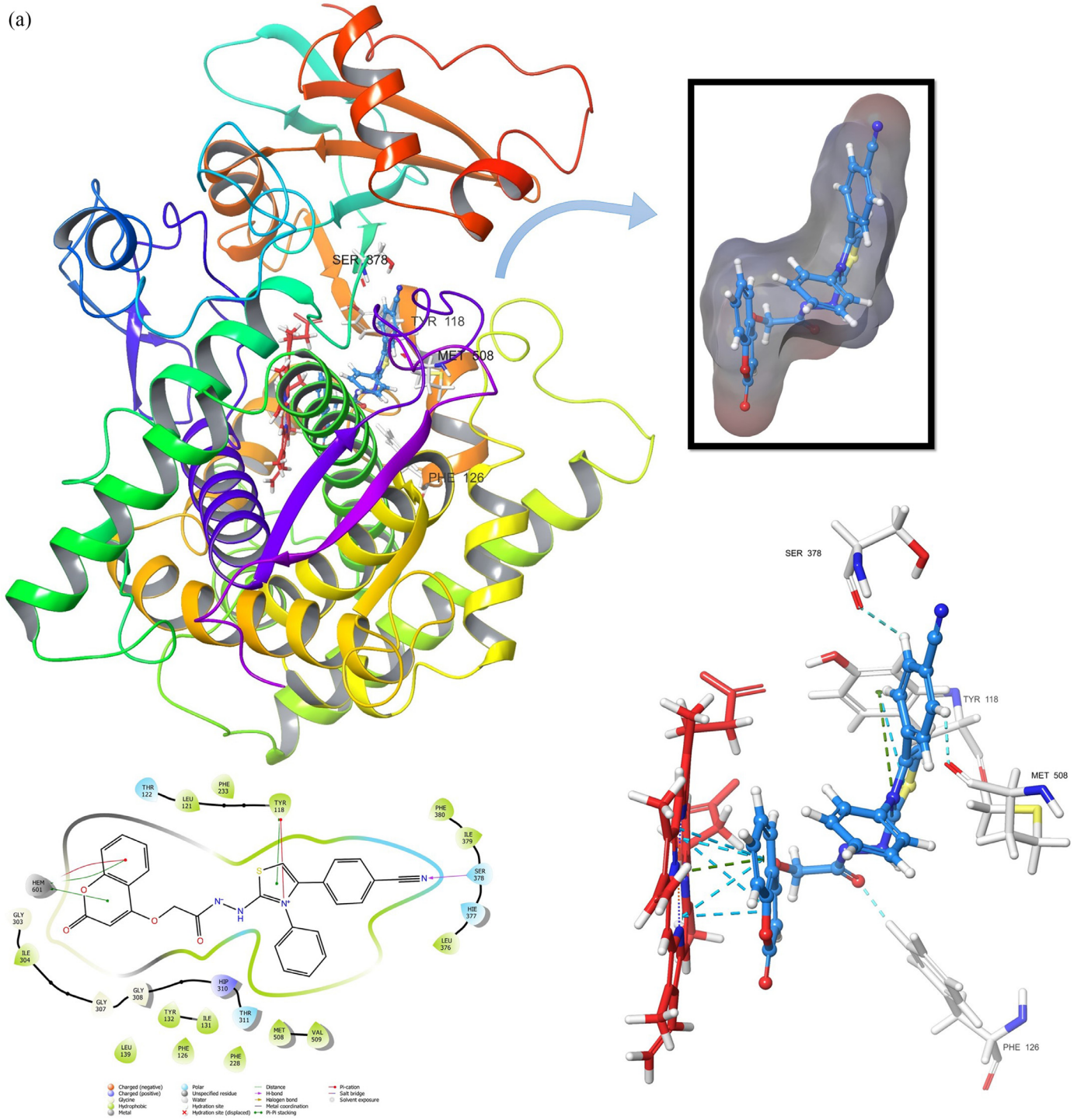

Fig. 1. **a**) Compound 4e in active pocket of lanosterol 14α-demethylase enzyme (PDBID: 5TZ1). Best pose is represented as 2D and 3D. In 3D pose, only interacted residues are displayed for clarity and the carbons of HEM protein are red, and the carbons of amino acids are white. **b**) Compound 4a (blue carbons) in the active pocket of thymidylate synthase (PDBID: 5J7W). The best pose is represented as 2D and 3D. In a 3D pose, only interacted residues are displayed for clarity, and the carbons of more important residues are red, while others are white. In superimposed representation, compound 4a's carbons are blue, and methotrexate's carbons are orange. Also, 2D structure of methotrexate was shared above the superposed representation.

thase (TS) from *E. faecalis* was selected as a potential specific target for antibacterial therapy [47]. Secondly, similar to methotrexate, the active compound includes one bicyclic ring (coumarin), a nitrogen-rich aliphatic chain (acyl hydrazide), and an aromatic ring (thiazole). And last, it has the same volume, shape, and length as methotrexate. We found that their spatial conformations clash in superimposed representation. For these reasons, we docked the active compounds into the active region of thymidylate synthase. Superimposed representation and docking pose are displayed in Fig. 1. Results revealed that there were one π-π stacking (Phe227), two H-bonds (Tyr145, Leu223), and 3 aromatic H-bonds (Trp81, Asp220, and Tyr260). All these amino acids were described previously as important active site residues [47], also compound **4e** has fit well in the enzyme active region, so its specific anti-E. faecalis activity is probably related to that. As a result, the docking study showed that our hypothesis is convenient. Moreover,

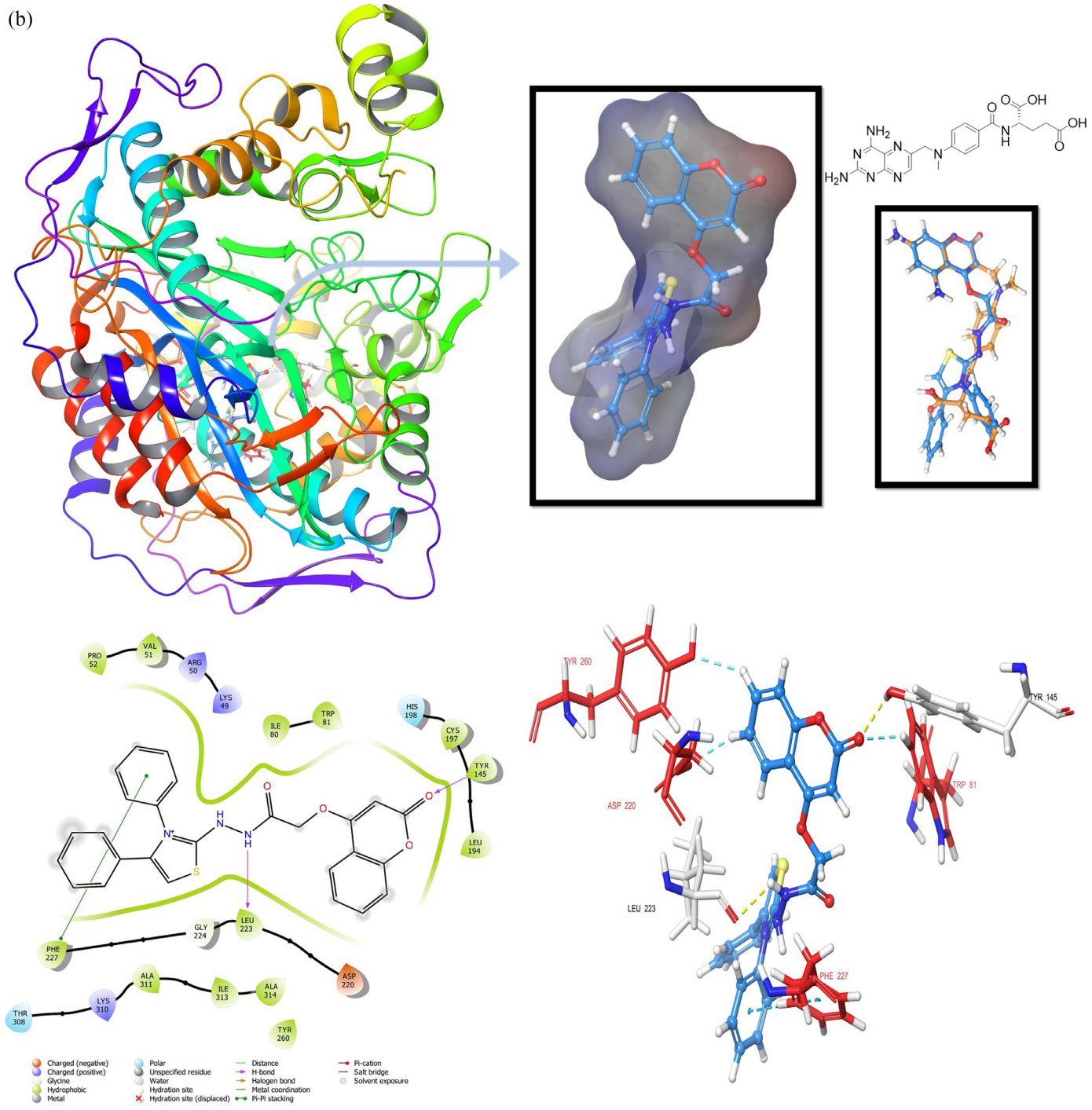

Fig. 1. Continued

the docking study suggested that 4th position substitutions are not favorable if they are bulky, in fact, 4-oxo- or nonsubstituted-thiazole may increase the inhibition activity because it can interact with amino acids in that cavity of the enzyme (such as Lys310 and Ala311). Additionally, the *N*-phenylthiazole group may be substituted with a hydrophilic but electron-donating group like *N*-(4-methoxyphenyl)thiazole, since it can result in forming H-bond with the solvents.

3.4.2. Molecular dynamics studies

The docking studies determined the possible activity mechanism, and also gave us an opinion to explain how it works. In this step, we tried to examine and understand the stability of the complex and its interaction strength over time.

In Fig. 2, the results are for the compound **4e**-14α-demethylase enzyme complex. According to them, the Rg plot showed atonic fluctuations of around 4.7 $\pm$ 0.3 Å, which are normal for the stable complexes. Between 87.50 and 94.70 ns, the fluctuations were a little more extreme, but still acceptable. This situation is probably related to the conformational change of the compound **4e**, but the stability was still preserved. Also, the RMSD values of the protein should be between 1 and 3 Å, they were calculated between 1.01 and 1.78 Å from 0.10 ns to the end of the simulation in this study. RMSF fluctuations of helix and strand structures were found

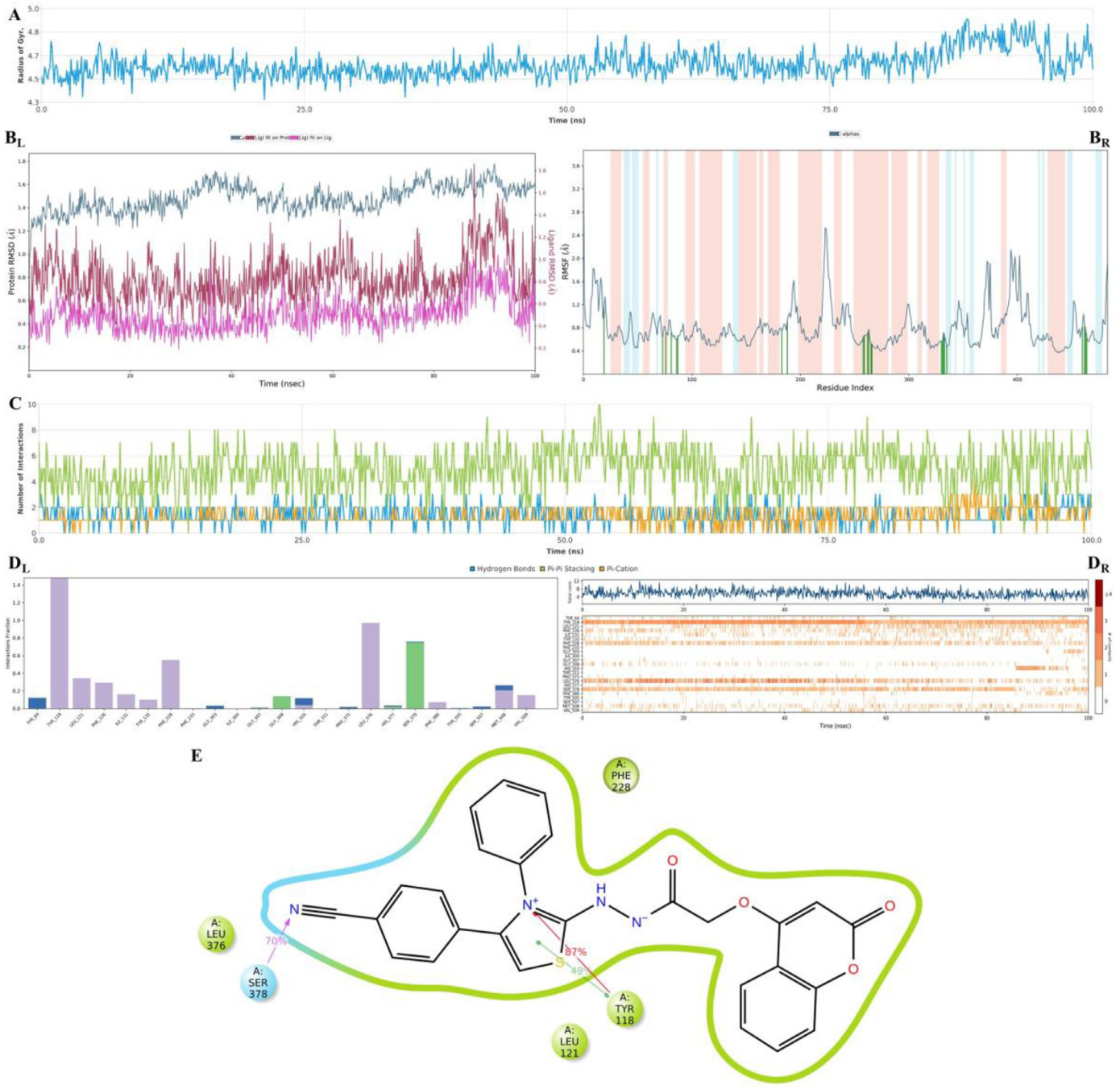

Fig. 2. MDS results of the compound 4e-14α-demethylase enzyme complex. The stability properties (Rg, RMSD, and RMSF plots, respectively.) are in the A-B sections; The interaction properties (C: Number of interactions-interaction types-time plot; D_L: Interaction fraction-residue diagram; DR..: Total connections-residues-time plot; E: 2D interaction pose with connection strength (cut off = 0.3) at the active region) are in the C-E sections.

to be minimal. On the other hand, RMSF fluctuations of the loop structure connected with the ligand were found to be minimal too. Hence, it revealed that the interaction with the ligand increased the stability of the ligand-protein complex. As a result, the stability properties of the complex were within an acceptable range. In Fig. 2 and video 1, all interactions and their types can be viewed. According to them, the dominant interactions are hydrophobic, H-bond, water-mediated H-bond, and aromatic H-bond interactions, respectively. Especially, the NH group of thiazolium moiety enabled π-cation interaction with Tyr118 amino acid, and its ring enabled π-π stacking with the same residue. These contacts are never cut off during simulation time. Additionally, H-bond forming was observed between nitrogen of the CN group and Ser378 amino acid. In video1, aromatic H-bonds were represented as faded teal dashes, and were seen between the ligand and Phe126, Tyr132, Phe228, Gly307, Thr311, Ser378, Met508, and Val509 amino acids. Interaction with Tyr118 increased the stability of the complex since it is continuous. Because of that, the MDS study points out that Tyr118 is the key residue for inhibition activity. After that, interactions with Phe226, Leu376, and Ser378 amino acids were determined as the most stable contacts. In fact, all these 3 residues were mentioned as important for inhibition activity in this study. On the other hand, even if the connections with Phe126, and Met508 were seen off and on during the simulation, it can be suggested

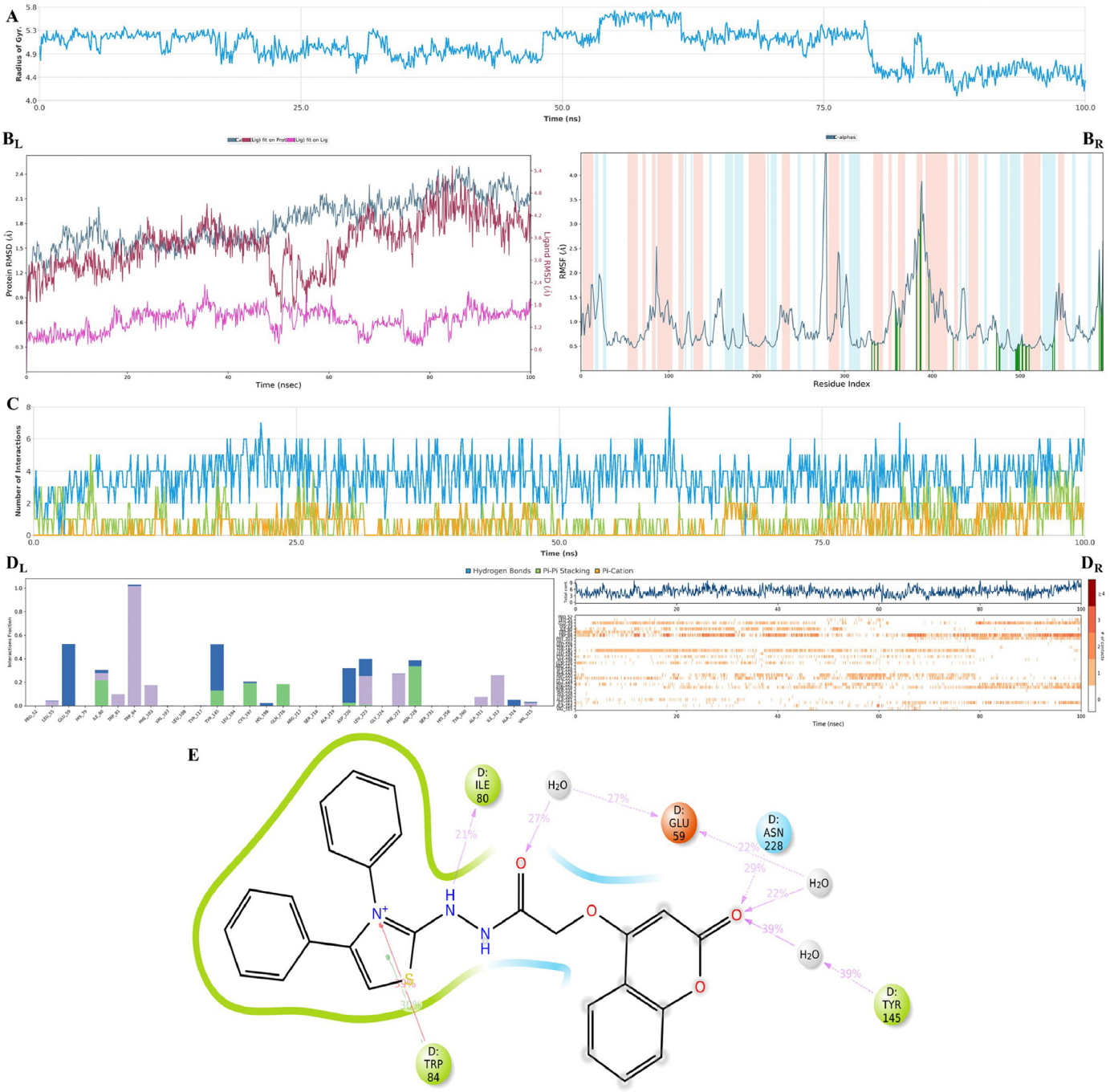

Fig. 3. MDS results of the compound 4a-thymidylate synthase complex. The stability properties (Rg, RMSD, and RMSF plots, respectively) are in the A-B sections; The interaction properties (C: Number of interactions-interaction types-time plot; D_L: Interaction fraction-residue diagram; D_R: Total connections-residues-time plot; E: 2D interaction pose with connection strength (cut off = 0.2) at the active region) are in the C-E sections.

that interacting with these residues increased the stability since these amino acids are members of the different loop regions. Similar to them, connections with Leu121 were seen once in a while during the simulation, and since this amino acid is a member of an α-helix, it encouraged the inhibition activity positively, which can be commended. In conclusion, MDS results showed that the compound **4e** can be used against the lanosterol 14α-demethylase (LDM) enzyme as an antifungal agent.

In Fig. 3, the results are for the compound **4a**-thymidylate synthase enzyme complex. The fluctuations in the Rg plot are a measure of compactness, a quantity expected to be largely constant for a protein with a stable tertiary structure. According to the results, it did not show drastic changes in this study, even though some jumps were seen partly during the simulation, so they are in the acceptable ranges. In fact, these jumps are related to solvent exposure, which affected the coumarin ring of the ligand. That is why water-mediated H-bonds with some polar amino acids (Glu59, and Tyr145) were formed in addition to direct H-bonds with Asn228. These bonds have increased the stability of the complex. Moreover, according to total connections-residues-time (Fig. 3-D_r) and RMSD (Fig. 3-B_r) plots, interaction with Glu59 residue has a major impact on the stability as hypothesized in its docking section. In the RMSF plot, the changes in fluctuations were observed largely at sites away from the ligand-binding region. Also, interaction with

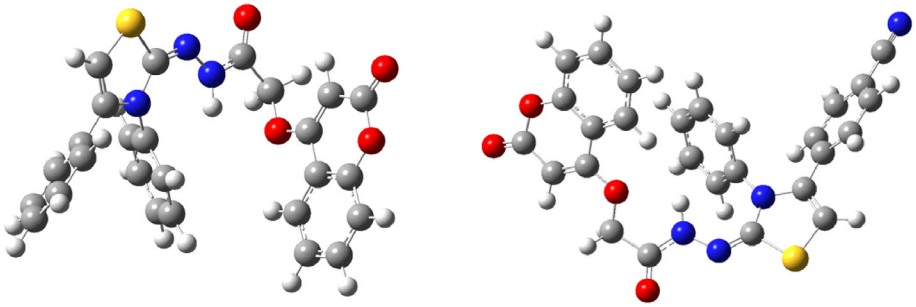

Fig. 4. Optimized molecular structures and total energy values of the active compounds.

loop residues resulted in their low RMSF values. Because these interactions were made with the loop amino acid, Tyr 145, it has increased both the stability of the complex and the inhibition activity, as seen in Fig. 3 and video2. In general, interactions with Glu59, Tyr84, Ile80, Tyr145, and Asp228 amino acids are remarkable, and their functions in their system complex and the activity were clarified in this paragraph.

Generally, *in silico* studies, the anticandidal and antibacterial activities of the active compound were explained, and their action mechanisms were studied. According to the results, coumarin-thiazole ring system hybridization via hydrazone link is a potential antimicrobial core structure. Especially, 3,4-disubstitutedthiazole moiety substantially influenced the type of activity and power of activity. Indeed, 4-(4-substitutedphenyl)thiazole derivatives did not show antibacterial activity as they could not stabilize an enzyme region due to their bulky shape and hydrophobic properties. On the contrary, 4-substituted phenyl groups have antifungal activity, especially, the hydrogen acceptor (cyano-) group. Thus, to obtain better antifungal activity, these substitutions will be modified with various hydrogen acceptors in further studies. As a pharmacophore structure, the coumarin ring has shown a good antimicrobial activity profile, and in this study, its structure-activity relationship (SAR) was explained through the enzyme active regions of 2 different organisms.

3.5. Theoretical

3.5.1. The theoretical geometry analysis and dipole moments

Molecular structures with total energy values of *N*'-(3,4-diphenylthiazol-2(3*H*)-ylidene)−2-((2-oxo-2*H*-chromen-4-yl)oxy)acetohydrazide derivatives **4a–4j** compounds were optimized using DFT/ B3LYP/6–31G(d,p) and the most active compounds are shown in Fig. 4, whereas Fig. S2 shows others (see Supplementary Material). The total energy values (Fig. 4 and Fig. S2) for the compounds **4a–4j** are ordered as follows: **4a** < **4f** < **4e** < **4b** < **4g** < **4i** < **4c** < **4d** < **4*h*** < **4j**. According to estimated total energy values of molecular structures, compounds with lower total energy values have a more stable structure.

The dipole moment is a measure of a molecule's polarity. Furthermore, the dipole moment was calculated at the DFT/B3LYP/6–31G(d,p) level using Eq. (1), and the results are shown in Table 4. The dipole moment of molecule **4a** indicates that it is more polarized, whereas molecule **4j** is less polarized.

3.5.2. Frontier molecular orbitals

HOMO-LUMO energy values, also known as frontier molecular orbital energies, are critical in estimating some reactivity characteristics of structures, especially in modeling studies involving molecular groups formed by different substituents. Given that a high HOMO energy value indicates a molecule structure's ability to donate electrons and a low LUMO energy value indicates a chemical structure's ability to accept electrons [48], it will be able to identify nucleophilic and electrophilic molecular groups. Moreover, the HOMO-LUMO (E) energy gap value gives information about molecular system stability and reactivity; structures with a small energy gap are thought to be less stable and reactive. Table 5. shows the calculated HOMO and LUMO, (ΔE) energy gap values for the **4a–4j** compounds. Table 5. shows that compound **4c** has the smallest energy gap (ΔE) with a value of 0.1071 eV, while compound **4b** has the biggest energy gap (E) with a value of 0.1386 eV, indicating that compound **4c** is more reactive and less stable than the others. Fig. 5 shows HOMO-LUMO orbital diagrams of active compounds, whereas Fig. S3 shows others (see Supplementary Material).

Table 4
The values of electric dipole moment of the **4a–4j** compounds.

Compounds	μ_x (Debye)	μ_y (Debye)	μ_z (Debye)	μ_{tot} (Debye)
4a	−6.0721	8.7949	4.3567	11.5413
4b	−0.8494	4.1068	3.4065	5.4029
4c	2.3664	−3.8536	2.2590	5.0550
4d	5.6807	−4.5115	1.1839	7.3502
4e	−3.4157	−2.3172	2.0693	4.6172
4f	−4.7313	−6.1616	2.4500	8.1457
4g	−3.2288	4.1074	4.8010	7.0955
4h	1.8404	1.4908	5.3172	5.8208
4i	−9.3539	−2.7433	1.8077	9.9141
4j	3.0495	0.3567	1.0444	3.2431

For specified compounds, **4a** with a low I value and **4i** with a high A value emerge as the most significant ionization potential (I) and electron affinity (A) values related to HOMO and LUMO energy. As a result, the **4a** compound has a nucleophilic character, whereas the **4i** molecule has an electrophilic character that is superior to the others. Electronegativity (χ) refers to an atom's proclivity to attract shared electrons (or electron density) to itself. The more electrons are attracted to an atom or a substituent group, the higher the related electronegativity. Electro-positivity is the polar opposite of electronegativity and measures a molecule's ability to give valence electrons. Compounds **4a–4j** have high χ with decreasing order of **4i** > **4c** > **4j** > **4e** > **4*h*** > **4d** > **4b** > **4f** > **4*g*** > **4a** and high ω values with decreasing order of **4i** > **4c** > **4e** > **4j** > **4d** > **4*h*** > **4b** > **4a** > **4f** > **4g**. As we see Compound **4i** with 0.2148 eV values has a higher electronegativity and with 0.2321 eV values has good electrophilic character than the others. According to the chemical hardness-softness (η, S) values, which are useful in assessing the intramolecular charge transfer of molecular structures, **4c** has a high S and a low η value.

Table 5
Some reactivity parameters of the compounds **4a–4j**.

Compounds	E_{HOMO} (eV)	E_{LUMO} (eV)	ΔE (eV)	I (eV)	A (eV)	χ (eV)	η (eV)	S (eV^{-1})	μ (eV)	ω (eV)
4a	−0.1869	−0.0587	0.1282	0.1869	0.0587	0.1228	0.0641	7.8003	−0.1228	0.1176
4b	−0.1971	−0.0585	0.1386	0.1971	0.0585	0.1278	0.0693	7.2150	−0.1278	0.1178
4c	−0.2100	−0.1029	0.1071	0.2100	0.1029	0.1564	0.0535	9.3458	−0.1564	0.2286
4d	−0.1926	−0.0645	0.1281	0.1926	0.0645	0.1285	0.0640	7.8125	−0.1285	0.1290
4e	−0.1985	−0.0764	0.1221	0.1985	0.0764	0.1374	0.0610	8.1967	−0.1374	0.1547
4f	−0.1910	−0.0573	0.1337	0.1910	0.0573	0.1241	0.0668	7.4850	−0.1241	0.1153
4 g	−0.1901	−0.0568	0.1333	0.1901	0.0568	0.1234	0.0666	7.5075	−0.1234	0.1143
4h	−0.1978	−0.0614	0.1364	0.1978	0.0614	0.1296	0.0682	7.3314	−0.1296	0.1231
4i	−0.2148	−0.1048	0.1100	0.2148	0.1048	0.1598	0.0550	9.0909	−0.1598	0.2321
4j	−0.2050	−0.0725	0.1325	0.2050	0.0725	0.1387	0.0662	7.5529	−0.1387	0.1453

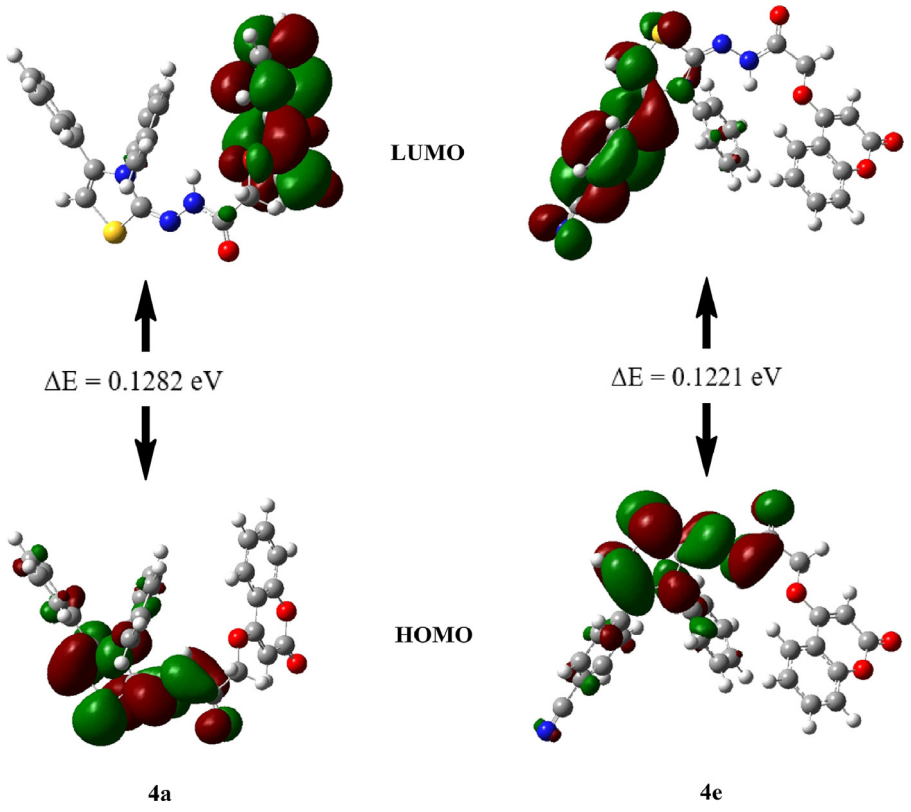

Fig. 5. HOMO-LUMO diagrams of the active compounds.

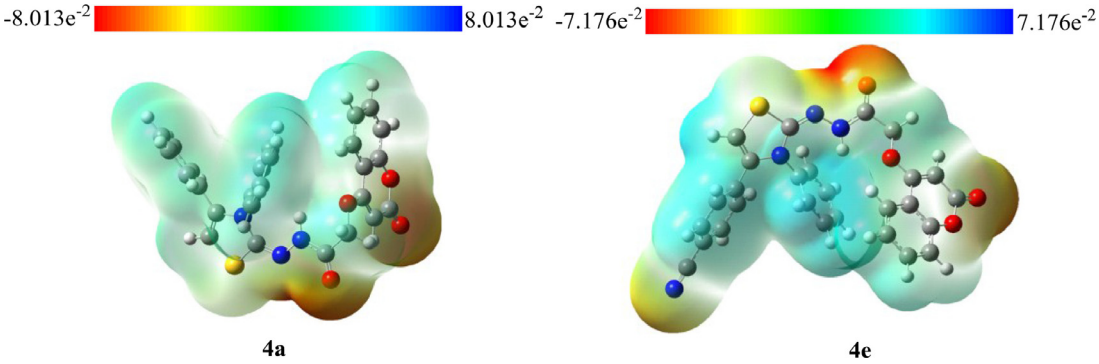

Fig. 6. Molecular electrostatic potential (MEP) surfaces presentation of the active compounds. The electrostatic potential (ESP) is given in Hartree atomic units (a.u.).

3.5.3. Molecular electrostatic potentials values (MEP)

The molecular electrostatic potential (MEP) at a certain point p(x,y,z) in the neighborhood of a molecule is the force acting on a positive test charge (a proton) positioned at p through the electrical charge cloud created by the molecule's electrons and nuclei. Despite the fact that the external test charge has no effect on the molecular charge distribution, the electrostatic potential of a molecule is an excellent guide in identifying a molecule's reactivity towards positively or negatively charged reactants (no polarization occurs) [49]. The MEP scheme reveals multiple colors: red indicates an electron-rich zone because of a partial negative charge, blue represents an electron-deficient zone because of a partial pos-

itive charge, yellow represents a moderately electron-rich zone, and green represents a neutral zone [50]. Fig. 6 shows the Molecular Electrostatic Potential (MEP) of active compounds, whereas Fig. S4 shows others (see Supplementary Material).

4. Conclusion

The synthesis and biological assessment of ten novel *N*'-(3,4-diphenylthiazol-2(3*H*)-ylidene)−2-((2-oxo-2*H*-chromen-4-yl)oxy)acetohydrazide derivatives (**4a–4j**) were described in this work. The resultant compounds' antibacterial activity was investigated. The investigation of their antimicrobial characteristics indicated that all substances have the capacity to inhibit the growth of various strains of bacteria and fungus to varying degrees. However, compounds **4c**, **4e**, and **4i** showed good activity against fungal strains. It was found that the antifungal activity of analogues was enhanced by nitro and cyano groups. Furthermore, a nitro group at the para position was more effective than meta substitution patterns. Those novel compounds have been demonstrated to be more effective against E. *coli* than any other gram-negative bacteria. In particular, the compound **4i** has stronger action against E. *coli* than other compounds. The activity against gram-positive bacteria is not high, except for E. *faecalis* bacteria, where compounds **4a** and **4j** exhibit strong activity, 1.95 µg / mL, and 3.90 µg / mL, respectively. Performing the molecular docking and molecular dynamics simulation studies, the action mechanism of the active compounds and also the structure-activity relationship were explained. Moreover, the chemical reactivity characteristics of all compounds were investigated using DFT. As a result of the DFT calculations, with potential most active molecule turns out to be **4a**, which really exhibits stronger antibacterial activity than the others.

Ethics approval and consent to participate

Not applicable.

Human and animal rights

Not applicable.

Consent for publication

Not applicable.

Availability of data and materials

The authors confirm that the data supporting the findings of this research are available along with the manuscript.

Declaration of Competing Interest

The authors declare that they have no known competing financial interests or personal relationships that could have appeared to influence the work reported in this paper.

CRediT authorship contribution statement

Demokrat Nuha: Conceptualization, Methodology, Software, Validation, Formal analysis, Investigation, Resources, Data curation, Writing – original draft, Visualization, Writing – review & editing. **Asaf Evrim Evren:** Conceptualization, Methodology, Software, Validation, Formal analysis, Investigation, Resources, Data curation, Writing – original draft, Visualization, Writing – review & editing. **Özge Kapusiz:** Methodology, Writing – review & editing. **Ülküye Dudu Gül:** Methodology, Writing – review & editing. **Nalan Gundogdu-Karaburun:** Validation, Resources, Writing – review & editing. **Ahmet Çagri Karaburun:** Conceptualization, Validation, Resources, Data curation, Writing – original draft, Supervision, Writing – review & editing. **Halil Berber:** Validation, Writing – review & editing.

Data availability

I have shared the data in the attached file step.

Funding

This research did not receive any specific grant from funding agencies in the public, commercial, or not-for-profit sectors.

Acknowledgments

We gratefully thank Anadolu University DOPNA Laboratory for analyzing the synthesized compounds.

Supplementary materials

Supplementary material associated with this article can be found, in the online version, at doi:10.1016/j.molstruc.2022.134166.

References

[1] M. Imran, K.R. Das, M.M. Naik, Co-selection of multi-antibiotic resistance in bacterial pathogens in metal and microplastic contaminated environments: an emerging health threat, Chemosphere 215 (2019) 846–857, doi:10.1016/j.chemosphere.2018.10.114.
[2] G. Karam, J. Chastre, M.H. Wilcox, J.L. Vincent, Antibiotic strategies in the era of multidrug resistance, Crit. Care 20 (2016) 136, doi:10.1186/s13054-016-1320-7.
[3] E. Meade, M.A. Slattery, M. Garvey, Bacteriocins, potent antimicrobial peptides and the fight against multi drug resistant species: resistance is futile? Antibiotics (2020) 9 (Basel), doi:10.3390/antibiotics9010032.
[4] S.D. Kumar, S.Y. Shin, Antimicrobial and anti-inflammatory activities of short dodecapeptides derived from duck cathelicidin: plausible mechanism of bactericidal action and endotoxin neutralization, Eur. J. Med. Chem. 204 (2020) 112580, doi:10.1016/j.ejmech.2020.112580.
[5] H.K. Allen, J. Trachsel, T. Looft, T.A. Casey, Finding alternatives to antibiotics, Ann. N. Y. Acad. Sci. 1323 (2014) 91–100, doi:10.1111/nyas.12468.
[6] M. Magana, M. Pushpanathan, A.L. Santos, L. Leanse, M. Fernandez, A. Ioannidis, M.A. Giulianotti, Y. Apidianakis, S. Bradfute, A.L. Ferguson, A. Cherkasov, M.N. Seleem, C. Pinilla, C. De La Fuente-Nunez, T. Lazaridis, T. Dai, R.A. Houghten, R.E.W. Hancock, G.P. Tegos, The value of antimicrobial peptides in the age of resistance, Lancet Infect. Dis. 20 (2020) e216–e230, doi:10.1016/s1473-3099(20)30327-3.
[7] R.E.W. Hancock, M.A. Alford, E.F. Haney, Antibiofilm activity of host defence peptides: complexity provides opportunities, Nat. Rev. Microbiol. 19 (2021) 786–797, doi:10.1038/s41579-021-00585-w.
[8] G. Maroti, A. Kereszt, E. Kondorosi, P. Mergaert, Natural roles of antimicrobial peptides in microbes, plants and animals, Res. Microbiol. 162 (2011) 363–374, doi:10.1016/j.resmic.2011.02.005.
[9] R.M. Epand, R.F. Epand, Domains in bacterial membranes and the action of antimicrobial agents, Mol. Biosyst. 5 (2009) 580–587, doi:10.1039/b900278m.
[10] C. Shao, Y. Zhu, Z. Lai, P. Tan, A. Shan, Antimicrobial peptides with protease stability: progress and perspective, Future Med. Chem. 11 (2019) 2047–2050, doi:10.4155/fmc-2019-0167.
[11] J. Nawrot-Modranka, E. Nawrot, J. Graczyk, *In vivo* antitumor, *in vitro* antibacterial activity and alkylating properties of phosphorohydrazine derivatives of coumarin and chromone, Eur. J. Med. Chem. 41 (2006) 1301–1309, doi:10.1016/j.ejmech.2006.06.004.
[12] Sh. Zhang, X. Tan, Ch. Liang, W. Zhang, Design, synthesis, and antifungal evaluation of novel coumarin-pyrrole hybrids, J. Het. Chem. 58 (2021) 450–458, doi:10.1002/jhet.4180.
[13] G. Yang, L. Shi, Z. Pan, L. Wu, L. Fan, C. Wang, C. Xu, J. Liang, The synthesis of coumarin thiazoles containing a trifluoromethyl group and their antifungal activities, Arab. J. Chem. 14 (2021) 102880, doi:10.1016/j.arabjc.2020.10.027.
[14] Y.K. Tyagi, A. Kumar, H.G. Raj, P. Vohra, G. Gupta, R. Kumari, P. Kumar, R.K. Gupta, Synthesis of novel amino and acetyl amino-4-methylcoumarins and evaluation of their antioxidant activity, Eur. J. Med. Chem. 40 (2005) 413–420, doi:10.1016/j.ejmech.2004.09.002.
[15] Z. Chen, J. Bi, W. Su, Synthesis and antitumor activity of novel coumarin derivatives via a three-component reaction in water, Chin. J. Chem. 31 (2013) 507–514, doi:10.1002/cjoc.201201130.
[16] A. Önder, Anticancer activity of natural coumarins for biological targets, 64 (2020) 85–109. 10.1016/b978-0-12-817903-1.00003-6

[17] J. Grover, S.M. Jachak, Coumarins as privileged scaffold for anti-inflammatory drug development, RSC Adv. 5 (2015) 38892–38905, doi:10.1039/c5ra05643h.
[18] F. Golfakhrabadi, M. Abdollahi, M.R. Ardakani, S. Saeidnia, T. Akbarzadeh, A.N. Ahmadabadi, A. Ebrahimi, F. Yousefbeyk, A. Hassanzadeh, M. Khanavi, Anticoagulant activity of isolated coumarins (suberosin and suberenol) and toxicity evaluation of Ferulago carduchorum in rats, Pharm. Biol. 52 (2014) 1335–1340, doi:10.3109/13880209.2014.892140.
[19] A.H. Gilani, F. Shaheen, S.A. Saeed, S. Bibi, M.S Irfanullah, S. Faizi, Hypotensive action of coumarin glycosides from Daucus carota, Phytomedicine 7 (2000) 423–426, doi:10.1016/s0944-7113(00)80064-1.
[20] Y.Q. Hu, Z. Xu, S. Zhang, X. Wu, J.W. Ding, Z.S. Lv, L.S. Feng, Recent developments of coumarin-containing derivatives and their anti-tubercular activity, Eur. J. Med. Chem. 136 (2017) 122–130, doi:10.1016/j.ejmech.2017.05.004.
[21] X. Wang, H. Zhou, X. Wang, K. Lei, S. Wang, Design, synthesis, and *in vivo* and *in silico* evaluation of coumarin derivatives with potential antidepressant effects, Molecules 26 (2021), doi:10.3390/molecules26185556.
[22] CLSI, Methods For Dilution Antimicrobial Susceptibility Tests For Bacteria That Grow aerobically; Approved Standard—Ninth edition. CLSI Document M07-A9., Clinical and Laboratory Standards Institute, Wayne, Pennsylvania, USA, 2012.
[23] A.E. Evren, S. Dawbaa, D. Nuha, Ş.A. Yavuz, Ü.D. Gül, L. Yurttaş, Design and synthesis of new 4-methylthiazole derivatives: *in vitro* and *in silico* studies of antimicrobial activity, J. Mol. Struct. 1241 (2021) 130692, doi:10.1016/j.molstruc.2021.130692.
[24] D. Nuha, A.E. Evren, M. Yilmaz Cankiliç, L. Yurttaş, Design and synthesis of novel 2,4,5-thiazole derivatives as 6-APA mimics and antimicrobial activity evaluation, Phosphorus Sulfur Silicon Relat. Elem. 196 (2021) 954–960, doi:10.1080/10426507.2021.1946537.
[25] A. Daina, O. Michielin, V. Zoete, iLOGP: a simple, robust, and efficient description of n-octanol/water partition coefficient for drug design using the GB/SA approach, J. Chem. Inf. Model. 54 (2014) 3284–3301, doi:10.1021/ci500467k.
[26] A. Daina, O. Michielin, V. Zoete, SwissADME: a free web tool to evaluate pharmacokinetics, drug-likeness and medicinal chemistry friendliness of small molecules, Sci. Rep. 7 (2017) 42717, doi:10.1038/srep42717.
[27] A.E. Evren, D. Nuha, S. Dawbaa, B.N. Saglik, L. Yurttas, Synthesis of novel thiazolyl hydrazone derivatives as potent dual monoamine oxidase-aromatase inhibitors, Eur. J. Med. Chem. 229 (2022) 114097, doi:10.1016/j.ejmech.2021.114097.
[28] S. Maestro, Version 10.6, in: LLC, New York, 2016.
[29] Schrödinger Release 2020-3, Desmond, in, Schrödinger, LLC, New York, NY, USA, 2020.
[30] D.D. Humphreys, R.A. Friesner, B.J. Berne, A multiple-time-step molecular dynamics algorithm for macromolecules, J. Phys. Chem. 98 (1994) 6885–6892.
[31] W.G. Hoover, Canonical dynamics: equilibrium phase-space distributions, Phys. Rev. A 31 (1985) 1695.
[32] G.J. Martyna, D.J. Tobias, M.L. Klein, Constant pressure molecular dynamics algorithms, J. Chem. Phys. 101 (1994) 4177–4189.
[33] U. Essmann, L. Perera, M.L. Berkowitz, T. Darden, H. Lee, L.G. Pedersen, A smooth particle mesh Ewald method, J. Chem. Phys. 103 (1995) 8577–8593.
[34] F.F. Silveira, J.O. De Souza, L.V. Hoelz, V.R. Campos, V.A. Jabor, A.C. Aguiar, M.C. Nonato, M.G. Albuquerque, R.V. Guido, N. Boechat, Comparative study between the anti-P. falciparum activity of triazolopyrimidine, pyrazolopyrimidine and quinoline derivatives and the identification of new PfDHODH inhibitors, Eur. J. Med. Chem. 209 (2021) 112941.
[35] M. Frisch, G. Trucks, H. Schlegel, G. Scuseria, M. Robb, J. Cheeseman, G. Scalmani, V. Barone, B. Mennucci, G. Petersson, Gaussian09, Revision A, in, Wallingford CT Inc., 2009, pp. 150–166.
[36] R. Dennington, T. Keith, J. Millam, GaussView, version 5, in, 2009.
[37] A.D. Becke, Density-functional thermochemistry. I. The effect of the exchange-only gradient correction, J. Chem. Phys. 96 (1992) 2155–2160, doi:10.1063/1.462066.
[38] D. Nuha, A.E. Evren, Z.S. Ciyanci, H.E. Temel, G. Akalin Ciftci, L. Yurttas, Synthesis, density functional theory calculation, molecular docking studies, and evaluation of novel 5-nitrothiophene derivatives for anticancer activity, Arch. Pharm. (2022) e2200105 (Weinheim), doi:10.1002/ardp.202200105.
[39] M. Jatczak, K. Muylaert, L.M. De Coen, J. Keemink, B. Wuyts, P. Augustijns, C.V. Stevens, Straightforward entry to pyrido[2,3-*d*]pyrimidine-2,4(1H,3H)-diones and their ADME properties, Bioorg. Med. Chem. 22 (2014) 3947–3956, doi:10.1016/j.bmc.2014.06.009.
[40] R. Arif, M. Rana, S. Yasmeen, M.S.K Amaduddin, M. Abid, M.S. Khan, Rahisuddin, facile synthesis of chalcone derivatives as antibacterial agents: synthesis, DNA binding, molecular docking, DFT and antioxidant studies, J. Mol. Struct. 1208 (2020) 127905, doi:10.1016/j.molstruc.2020.127905.
[41] F.A. Khan, R.H. Patil, D.B. Shinde, J.N. Sangshetti, Bacterial peptide deformylase inhibition of cyano substituted biaryl analogs: synthesis, *in vitro* biological evaluation, molecular docking study and *in silico* ADME prediction, Bioorg. Med. Chem. 24 (2016) 3456–3463, doi:10.1016/j.bmc.2016.05.051.
[42] Y. Isyaku, A. Uzairu, S. Uba, Computational studies of a series of 2-substituted phenyl-2-oxo-, 2-hydroxyl- and 2-acylloxyethylsulfonamides as potent antifungal agents, Heliyon 6 (2020) e03724, doi:10.1016/j.heliyon.2020.e03724.
[43] A. Arshad, H. Osman, M.C. Bagley, C.K. Lam, S. Mohamad, A.S. Zahariluddin, Synthesis and antimicrobial properties of some new thiazolyl coumarin derivatives, Eur. J. Med. Chem. 46 (2011) 3788–3794, doi:10.1016/j.ejmech.2011.05.044.
[44] M. Basanagouda, K. Shivashankar, M.V. Kulkarni, V.P. Rasal, H. Patel, S.S. Mutha, A.A. Mohite, Synthesis and antimicrobial studies on novel sulfonamides containing 4-azidomethyl coumarin, Eur. J. Med. Chem. 45 (2010) 1151–1157, doi:10.1016/j.ejmech.2009.12.022.
[45] N.M. Sabry, H.M. Mohamed, E.S. Khattab, S.S. Motlaq, A.M. El-Agrody, Synthesis of 4H-chromene, coumarin, 12H-chromeno[2,3-*d*]pyrimidine derivatives and some of their antimicrobial and cytotoxicity activities, Eur. J. Med. Chem. 46 (2011) 765–772, doi:10.1016/j.ejmech.2010.12.015.
[46] T.Y. Hargrove, L. Friggeri, Z. Wawrzak, A. Qi, W.J. Hoekstra, R.J. Schotzinger, J.D. York, F.P. Guengerich, G.I. Lepesheva, Structural analyses of Candida albicans sterol 14alpha-demethylase complexed with azole drugs address the molecular basis of azole-mediated inhibition of fungal sterol biosynthesis, J. Biol. Chem. 292 (2017) 6728–6743, doi:10.1074/jbc.M117.778308.
[47] A. Catalano, R. Luciani, A. Carocci, D. Cortesi, C. Pozzi, C. Borsari, S. Ferrari, S. Mangani, X-ray crystal structures of enterococcus faecalis thymidylate synthase with folate binding site inhibitors, Eur. J. Med. Chem. 123 (2016) 649–664, doi:10.1016/j.ejmech.2016.07.066.
[48] K. Fukui, Role of frontier orbitals in chemical reactions, Science 218 (1982) 747–754, doi:10.1126/science.218.4574.747.
[49] P. Politzer, J.S. Murray, The fundamental nature and role of the electrostatic potential in atoms and molecules, Theor. Chem. Acc. Theory Comput. Model. (Theor. Chim. Acta) 108 (2002) 134–142, doi:10.1007/s00214-002-0363-9.
[50] F.J. Luque, M. Orozco, P.K. Bhadane, S.R. Gadre, SCRF calculation of the effect of water on the topology of the molecular electrostatic potential, J. Phys. Chem. 97 (2002) 9380–9384, doi:10.1021/j100139a021.